Polymer Degradation and Stability 222 (2024) 110710

Contents lists available at ScienceDirect

Polymer Degradation and Stability

journal homepage: www.journals.elsevier.com/polymer-degradation-and-stability

Impact of thermomechanical reprocessing on multilayer plastic packaging blend

Ke Zhan [a], Daniel Meadows [b], Lindsay Levy [c], Raymond Hou [c], Tanmay Rahman [b], Virginia Davis [b], Edward Davis [b], Bryan S. Beckingham [b], Brian Via [a], Thomas Elder [d], Yucheng Peng [a,*]

[a] College of Forestry, Wildlife and Environment, Auburn University, Auburn, AL 36849, USA
[b] Samuel Ginn College of Engineering, Auburn University, Auburn, AL 36849, USA
[c] Loveless Academic Magnet Program High School, Montgomery, AL 36111, USA
[d] USDA-Forest Service, Southern Research Station, Auburn, AL 36849, USA

ARTICLE INFO

Keywords:
Multilayer plastic packaging
Thermomechanical reprocessing
Mechanical properties
Rheological properties
Cross-linking
EVOH gelling

ABSTRACT

Multilayer plastic packaging (MPP) has attracted extensive attention due to its functionality and inherent difficulty in reclamation. One primary concern is the performance of reprocessed MPP since it inherently consists of many dissimilar polymers. This study aims to assess the effect of multiple thermomechanical reprocessing cycles on the properties of a MPP blend. Low density polyethylene (LDPE)/maleic anhydride grafted linear LDPE (LLDPE-g-MA)/ethylene vinyl alcohol (EVOH) blend was manufactured and subjected to thermomechanical reprocessing, including thermal compounding, grinding, and injection molding for six cycles to characterize the impact of thermomechanical reprocessing on the blend's mechanical, morphological, thermal, and rheological properties. The tensile strength and modulus of the reprocessed blend remained consistent throughout six cycles. A pronounced decline in elongation at break was observed after four cycles of reprocessing. Toughness, as represented by the essential work of fracture, increased steadily up to three cycles of processing, followed by a decline in the following reprocessing cycles. The main property change is possibly caused by the gelling of the EVOH in the reprocessed blend, as demonstrated by larger EVOH agglomerates in the LDPE matrix. Differential scanning calorimetry results indicated that the degree of crystallization of the EVOH phase changed with increasing reprocessing cycles, suggesting EVOH degradation. Rheological behavior in the linear viscoelastic region indicated enhanced interfacial interaction between LDPE and EVOH due to the cross-linking of LLDPE-g-MA and rigid EVOH in the early reprocessing stages. After four cycles of reprocessing, decreases in storage and loss moduli were observed, indicating the possibility of phase separation caused by gelling of EVOH. Using polymer blending to reclaim LDPE-based EVOH multilayer is promising for up to four cycles of reprocessing as shown by mechanical, thermal, and rheological behaviors.

1. Introduction

Multilayer plastic packaging (MPP) is an essential packaging material that synergistically integrates the merits of individual polymer layers, offering superior barrier effectiveness, robust mechanical resilience, and specialized features such as surface printability, chemical inertness, and high-temperature resistance [1]. Owing to its adaptability, multifunctionality, and ease of use, MPP has gained considerable attention recently and its utilization is expected to continue growing in the future [2]. Currently, packaging accounts for approximately 39.6 % of global plastic usage, making it the largest of all end-use sectors. Of this, 17 % is dedicated to MPP production, primarily for food packaging applications [3]. In most cases, multilayer configurations for food packaging typically consist of two outer layers of commodity polyolefins, mainly polypropylene (PP) or polyethylene (PE), and a central layer of barrier resins like ethylene vinyl alcohol (EVOH) or polyamide (PA). Tie resins serve as binding agents, combining these layers into a cohesive minimum five-layer structure [4]. Annually, over one hundred million tons of multilayer thermoplastics are produced worldwide [5]. With the growing use of MPP, there has been a notable rise in

* Corresponding author.
E-mail address: yzp0027@auburn.edu (Y. Peng).

https://doi.org/10.1016/j.polymdegradstab.2024.110710
Received 15 December 2023; Received in revised form 3 February 2024; Accepted 17 February 2024
Available online 17 February 2024

post-consumer waste and manufacturing scrap, emphasizing the importance of sustainable management and recycling strategies.

A series of methods [6–8] have been reported to address plastic waste issues, among which mechanical recycling is the predominant approach for managing post-industrial and post-consumer plastic wastes. However, this approach generally leads to irreversible changes to the polymer's physicochemical properties and structure due to exposure to elevated temperatures, high pressures, and applied shear forces during reprocessing, such as thermal compounding, injection molding, extrusion, and blow molding [9–13]. These changes result in significant polymer degradation, compromising its structural integrity and potentially diminishing its functional properties. Moreover, the exposure of recycled plastics to oxygen during reprocessing, along with the presence of moisture or residual contaminants, can cause thermo-oxidative degradation [14–16].

Saikrishnan et al. [17] studied the thermomechanical degradation of a PP and low density PE (LDPE) (PP/LDPE) blend during a simulated recycling process involving five cycles of twin-screw extrusion. This process led to chain scission in the PP phase, resulting in reduced viscosity, disrupted crystal structure, and slightly declined tensile properties. LDPE was also exposed to one hundred extrusion cycles to simulate mechanical recycling, as conducted by Jin et al. [18]. This simulated recycling had a minimal impact on the melting and crystallization temperatures. While analyses from rheological assessments, crystallinity, creep tests, and molecular weight (MW) measurements revealed that LDPE experienced thermal degradation and gelation after extensive extrusion, the repeated processes triggered simultaneous chain scission and cross-linking. Other studies [19–22] also revealed the degradation of various polymers under different reprocessing techniques, with a particular focus on investigating the evolution of polymers through multiple reprocessing cycles.

Although extensive works have been conducted to evaluate the influences of various reprocessing techniques on the properties of recycled polymers and elucidate polymer degradation mechanisms, limited attention has been focused on assessing how reprocessing impacts the properties of MPP and its recycled blend. Lahtela et al. [23] examined the properties of both rigid and flexible MPP materials reprocessed through crushing and injection molding. This study showed that the properties of recycled MPP were primarily determined by its primary matrix materials, highlighting the significance of sorted collection in future recycling efforts. However, sorting and recycling MPP is challenging due to the problematic separation of the packaging components, and large-scale industrial solutions for this issue are still lacking [24–26]. Considering MPP's complex structure and difficulty in separating the components, polymer blending emerges as a more feasible strategy for MPP reuse [27,28]. Polymer blending provides a simple, adaptable, and cost-effective approach to creating materials with enhanced properties [29].

Huang et al. [30] determined the properties of a LDPE/EVOH blend with LLDPE-g-MA added as a compatibilizer. Improved dispersion of the EVOH minor phase within the LDPE matrix was observed, accompanied by stable melting and crystallization behavior. An optimal compatibilizer content of one part per hundred of resin remarkably improved the tensile strength, modulus, and tear strength. Similarly, the effect of the LLDPE-g-MA compatibilizer on the crystallization, rheological, and tensile properties of a LDPE/EVOH blend was evaluated by Lee et al. [31]. The crystallization of the EVOH phase was retarded due to the formation of EVOH grafted LLDPE and a decrease in the EVOH domain size. However, the compatibilized blend exhibited increased complex viscosity, storage modulus, tensile strength, and elongation at break, owing to the improved interfacial adhesion promoted by LLDPE-g-MA. Moreover, Touil et al. [32] conducted a laboratory-scale recycling study in which a blend of LDPE, maleic anhydride grafted linear LDPE (LLDPE-g-MA), and EVOH was subjected to extrusion and injection molding processes. The work determined how the EVOH content, the ethylene content in EVOH, and extrusion temperature influence the compatibility of the blend. The results uncovered that enhanced compatibility, facilitated by LLDPE-g-MA, contributed to increased tensile strength. Increasing the EVOH content in the injection molded blend enhanced its tensile properties, and a higher compounding temperature further contributed to greater tensile strength. Meanwhile, increased amounts of EVOH and LLDPE-g-MA resulted in a reduction in the crystallinity of PE in the blend.

These studies suggest the potential of transforming an EVOH-based MPP into a polymer blend that exhibits superior mechanical performance. Fortuitously, the native tie layer in recycled MPP can serve as a compatibilizer, reducing cost compared to other polymer blends that require additional modifiers to enhance interfacial adhesion between polyolefins and EVOH. A newly published study by Cabrera et al. [33] further confirmed the concept of valorizing post-consumer MPP through polymer blending. In their study, the LLDPE-g-MA tie layer resin enhanced the interfacial adhesion between LLDPE and EVOH via a chemical reaction between the LLDPE-g-MA and EVOH.

Under optimal conditions, a one-time reprocessing appears to enhance the mechanical properties of the recycled MPP blend. Assessing the consistency of this improvement can offer valuable insights for refining the recycling process and expanding the application of recycled MPP. High temperature and shear forces during the repeated polymer melt compounding and subsequent reprocessing, such as injection molding and grinding, may potentially lead to polymer degradation in the reclaimed MPP blend. Therefore, investigating the impact of multiple reprocessing cycles on the properties of MPP blend is of great concern for effectively and sustainably recycling post-consumer MPP. Furthermore, understanding the degradation mechanisms during multiple recycling procedures is essential for enhancing performance and prolonging the lifespan of recycled MPP. More attention is urgently needed to promote development in this field.

In this study, we are focusing on an LDPE-based multilayer structure with EVOH as the barrier resin and LLDPE-g-MA as the tie resin. The primary objective is to evaluate the impact of multiple thermomechanical reprocessing on the MPP blend and to explore the feasibility of its recycling by employing polymer blending techniques. Mechanical, morphological, spectroscopic, thermal, and rheological properties were studied to elucidate the transformations of the reprocessed MPP that occur at the molecular and macroscopic levels during the repeated mechanical recycling.

2. Materials and methods

2.1. Materials

Commercial LDPE (density: 0.925 g/cc, melt index: 0.8 g/min at 190 °C/2.16 kg), LLDPE-g-MA (density: 0.930 g/cc, melt index: 2.5 g/min at 190 °C/2.16 kg) and EVOH (density: 1.190 g/cc, melt index: 3.2 g/min at 190 °C/2.16 kg, ethylene content: 32 mol.%) pellets were supplied by Berry Global, Inc. All pellets were dried in a forced air oven (Model 52411-11, Cole-Parmer Inc., Vernon Hills, IL, US) overnight at 80 °C to remove moisture before being used.

2.2. Thermomechanical reprocessing

2.2.1. Thermal compounding

LDPE, LLDPE-g-MA, and EVOH pellets were mixed to formulate a mixture that simulates recycled MPP. This mixture was subjected to thermal compounding, mechanical grinding, and injection molding under the same conditions for six cycles (termed Cycle 1 to Cycle 6) to simulate thermomechanical reprocessing used in practical polymer recycling and reuse.

Thermal compounding was conducted using an internal bowl mixer (Model 2128, C.W. Brabender Instruments, Inc., Hackensack, NJ, US) equipped with two counter-rotating roller blades. LDPE (70 wt.%), LLDPE-g-MA (20 wt.%), and EVOH (10 wt.%) pellets, one of the

representative compositions for high barrier commercial MPP, were dry blended manually before thermal compounding. The mixer was heated for approximately 15 min after reaching the desired operating temperature to ensure stable temperature conditions. A 200 g mixture was prepared and gradually added into the mixing chamber. The thermal compounding temperature, time, and counter-rotating speed were 200 °C, 5 min, and 60 rpm. The mixing torque value was observed and recorded until a stable value was obtained. After melt compounding, the resultant blend was scraped off the mixer using a scraper in its molten state and then allowed to solidify under room conditions.

2.2.2. Mechanical grinding

The solidified LDPE/LLDPE-g-MA/EVOH blend was ground into particles using a low-speed granulator (Model SG-2042NH, Shini Plastic Technologies, Inc., Willoughby, OH, US) with a 3 mm sieve size. The particles were dried in an oven overnight at 80 °C to eliminate moisture prior to being injection molded into standard specimens for subsequent mechanical testing and other characterizations.

2.2.3. Injection molding

A benchtop injection molding machine (Proto-Ject 150 HP, Manning Innovations, Inc., Halls, TN, US) was employed to manufacture testing specimens via two customized aluminum molds. Tensile testing samples were injection molded using a preheated mold (180 °C, 10 min) with a dimension of 101.6 mm (length) × 20 mm (width) × 0.98 mm (thickness) at 235 °C under a pressure of 57 MPa. The samples for the essential work of fracture (EWF) test were produced in dimensions of 63.5 mm (length) × 12.7 mm (width) × 3.2 mm (thickness) at 200 °C under a pressure of 51 MPa. A neat LDPE sample was prepared through injection molding without additional reprocessing for comparison purposes. All samples were stored in Ziploc bags to avoid moisture intrusion prior to characterization.

2.3. Characterizations

2.3.1. Tensile test

Tensile testing was performed using a universal testing machine (Model ESM750S, Mark-10, Copiague, NY, US) with a motorized test stand and a load cell of 500 N. Tensile properties were determined according to ASTM 882-12 standard [34]. The tensile testing samples with dimensions of 101.6 mm (length) × 15 mm (width) × 0.98 mm (thickness) were cut from injection molded samples using a razor blade. The testing speed and initial strain rate were set at 50 mm/min and 1 min^{-1}, respectively. Five duplicates were tested for each sample with error bars indicating standard deviation. One-way analysis of variance (ANOVA) statistical analysis of the tensile properties was performed using IBM SPSS software, and a significance level of $\alpha = 0.05$ was used. After the ANOVA analysis, a post-hoc test using Tukey's Honestly Significant Difference test was applied to assess the effect of different levels of the reprocessing cycle factor.

2.3.2. EWF test

The EWF method is increasingly recognized and utilized for characterizing the toughness of ductile polymers, toughened polymer blends, and composites [35–40]. The underlying concept of the EWF method, first proposed by Broberg [41] in 1968, assumes that the non-elastic region at the crack tip can be divided into an inner fracture process zone and an outer plastic deformation zone. Accordingly, the energy associated with the fracture of a viscoelastic material can be divided into two distinct parts: the EWF and the non-EWF. Several key correlations within the EWF concept are as follows [39,42,43]:

$$W_f = W_e + W_p$$

$$W_e = w_e tL$$

$$W_p = \beta w_p tL^2$$

$$w_f = \frac{W_f}{tL} = w_e + \beta w_p L$$

where W_f is the total work of fracture; L is the ligament length; t is the specimen thickness; W_e and W_p are EWF and non-EWF terms, which are proportional to the ligament area (tL) and the volume of yield zone (tL^2), respectively; w_f is the specific total work of fracture; w_e and w_p are the specific EWF and specific non-EWF, respectively; β is the shape factor related to the volume of the plastic deformation zone. For a given thickness, w_e represents a material constant that can be employed to characterize the fracture toughness [44], while βw_p is related to a material's resistance against crack propagation [45]. The values of w_e and βw_p can be obtained from the intercept and slope respectively in a linear regression between w_f and L [46].

The EWF test was conducted using the same universal testing machine and load cell as those used in the tensile test. The EWF samples were notched into the double-edge notched tension (DENT) specimens using a manual notching machine (CEAST, Instron, Norwood, MA, US) equipped with a blade (angle: 45 ± 1°, radius: 0.5 ± 0.05 mm). The geometry of the DENT specimen is depicted in Fig. 1 with the notching direction being perpendicular to the direction of the tensile load. The EWF tests were performed at room temperature with a constant crosshead speed of 5 mm/min. The testing length was 30 mm, while the ligament length varied from 4 to 8 mm. The accurate ligament length was measured using a trinocular stereo zoom microscope (Model 420T-430PHF-10, National Optical & Scientific Instruments Inc., Schertz, TX, US) with a Moticam digital camera as an accessory. Fifteen specimens were measured for each sample to ensure data reproducibility. The load-displacement curves were recorded, and the fracture energy was calculated from the area under the curves by numerical integration.

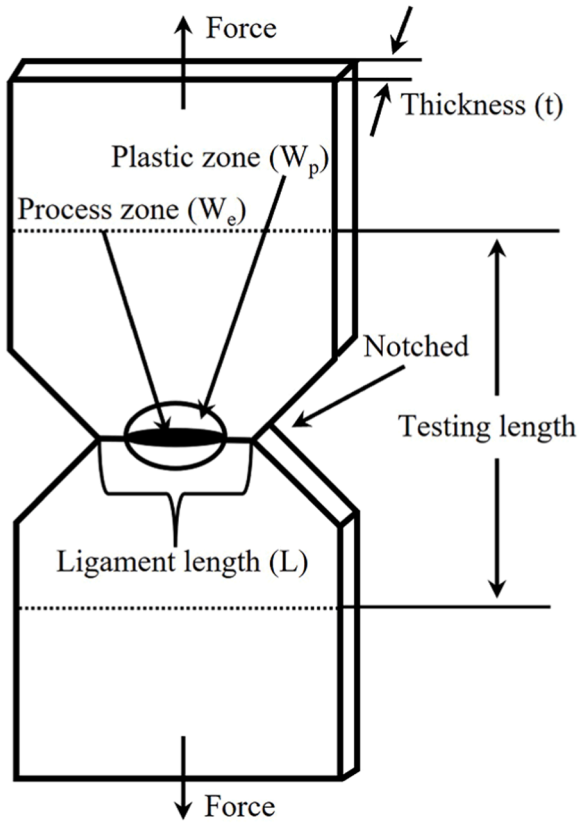

Fig. 1. Geometry of DENT specimen.

2.3.3. Morphology

The cross-sections of the EWF samples, which had not yet been notched and tested, were cut using a razor blade and observed through scanning electron microscopy (SEM, EVO 50, Zeiss, Oberkochen, Germany) at an accelerating voltage of 20 kV. The cross-sections were sputter-coated with gold for 60 s in a sputter-coating device (Q150R, Electron Microscopy Sciences, Hatfield, PA, US) before the SEM examination to enhance conductivity.

2.3.4. Fourier-transform infrared spectroscopy

LDPE, LLDPE-g-MA, EVOH, and the reprocessed blend were analyzed using Fourier-transform infrared spectroscopy (FTIR, Spotlight 400, PerkinElmer, Waltham, MA, US). An attenuated total reflection accessory with diamond/ZnSe crystals was employed. The transmittance was recorded from 650 to 4000 cm^{-1} with a resolution of 4 cm^{-1}. Sixty-four scans per spectrum were performed, and three duplicates were determined for each sample.

2.3.5. Thermal properties

The melting and crystallization behaviors of LDPE, LLDPE-g-MA, EVOH, and their reprocessed blend were characterized through differential scanning calorimetry (DSC, Q100, TA Instruments, New Castle, DE, US). An amount ranging from 7 to 9 mg of the samples was placed in the DSC under a nitrogen atmosphere with a flow rate of 50 mL/min. The samples were initially heated from 30 °C to 210 °C at a rate of 10 °C/min and then maintained at this temperature for 5 min to erase the thermal history. Subsequently, the samples were cooled to 30 °C at a rate of 10 °C/min for collecting crystallization data, followed by a second heating to 210 °C at the same rate of 10 °C/min to observe the melting behavior. The crystallization onset temperature (T_c-*onset*), peak temperature (T_c), and enthalpy (ΔH_c) were determined from the cooling scan, whereas the melting onset temperature (T_m-*onset*), peak temperature (T_m), and enthalpy (ΔH_m) were derived from the second heating scan. Three duplicates were examined for each sample. The degree of crystallinity (X_c) was calculated according to the following equation [47,48]:

$$X_c(\%) = \frac{1}{wt.\%}\left[\frac{\Delta H_m}{\Delta H_{m0}}\right] \times 100$$

where ΔH_m is the melting enthalpy of LDPE, LLDPE-g-MA, or EVOH; ΔH_{m0} is the melting enthalpy for a 100 % crystalline sample; and *wt.%* represents the weight fraction of the individual component in the blend. The value of ΔH_{m0} for 100 % crystalline PE was assumed to be 290 J/g [49]. The ΔH_{m0} for 100 % crystalline EVOH was calculated according to the following equation [50,51]:

$$\Delta H_{m0}^{EVOH} = \alpha \Delta H_{m0}^{PVA} + \beta \Delta H_{m0}^{PE}$$

where $\Delta H_{m0}{}^{PVA}$ is the melting enthalpy for 100 % crystalline poly(vinyl alcohol) (PVA) and was taken as 161.1 J/g [52]; $\Delta H_{m0}{}^{PE}$ is the same as above (290 J/g); and α and β are the mole fraction of vinyl alcohol and ethylene in EVOH, which is $\alpha = 0.68$ and $\beta = 0.32$ respectively in this work. The ΔH_{m0} for a 100 % crystalline EVOH was calculated as 202.4 J/g in this work.

2.3.6. Rheological properties

Rheological strain sweep and frequency sweep tests of LDPE and the reprocessed blend were conducted using a rheometer (MCR 302e, Anton Paar, Graz, Austria) equipped with a convection temperature device (CTD 450, Anton Paar, Graz, Austria). A parallel plate geometry with a diameter of 25 mm and a gap of 1 mm was used. The linear viscoelastic region (LVR) was determined by the strain sweep tests at a frequency of 10 rad/s. The strain was selected around five data points back from 5 % overall change in storage modulus to ensure all frequency tests are well within the LVR. Frequency sweep tests were conducted within the LVR with an angular frequency range from 0.1 to 582 rad/s to obtain viscoelastic properties as functions of frequency, including storage and loss moduli, complex viscosity, and phase angle. Time sweep tests of LDPE and the reprocessed blend were conducted using a rheometer (HAAKE MARS 60, Thermo Fisher Scientific, Germany) equipped with a parallel plate geometry (diameter = 25 mm, gap = 1.3 mm). The circular specimens with a diameter of 22 mm and a thickness of 1.5 mm were prepared using a Gasket punch (General Tools, Cincinnati, OH, US). The storage modulus values as a function of time were recorded over 30 min at a constant strain of 1 % and an angular frequency of 10 rad/s. All rheological tests were measured at 200 °C, and data were averaged over three trials with error bars to indicate standard deviation.

3. Results and discussion

3.1. Mechanical properties

The representative stress-strain curves of LDPE and the blend after each reprocessing cycle are provided in Fig. 2. The LDPE sample exhibited pronounced yielding and necking behaviors because of its branched polymer structure which endows the material with notable flexibility and facilitates significant plastic deformation under stress. The yielding occurred at a tensile stress close to 10 MPa, followed by necking, marked by a decrease in tensile stress. Strain hardening was observed where the tensile stress increased after necking, resulting from the alignment of polymer chains in the direction of stress, thereby contributing to an increase in hardness and strength.

The blend did not exhibit necking characteristics, indicating greater rigidity compared to neat LDPE, as EVOH is inherently much more rigid than LDPE. A higher tensile strain was found for the blend in Cycle 1 compared to that of neat LDPE, with the dispersed EVOH particles helping to carry more load and allowing the material to deform more before failure. The strain increased again when the blend was reprocessed into Cycle 2. This increase in tensile strain benefited from the enhanced interfacial adhesion, which resulted from a greater degree of reaction between LLDPE-g-MA and EVOH, contributing to more effective stress transfer. A similar tensile strain at break to that in Cycle 2 was found for the blend in Cycle 3. Subsequently, a marked decrease in the tensile strain at break was observed for the blend after reprocessing in Cycle 4, and it continuously decreased with the increase of cycle numbers. This can be attributed to an excessive interaction between LLDPE-g-MA and EVOH, which caused the EVOH particles to gel and increase in size, leading to more phase separation. After the Cycle 6 reprocess, the tensile strain at break was slightly lower than that of neat LDPE, but the tensile strength was still greater than LDPE. Moreover, as displayed in the insert, the color of the reprocessed blend became darker with the increase of reprocessing cycle numbers, which probably indicates a thermo-oxidative degradation [53]. This darkening in color

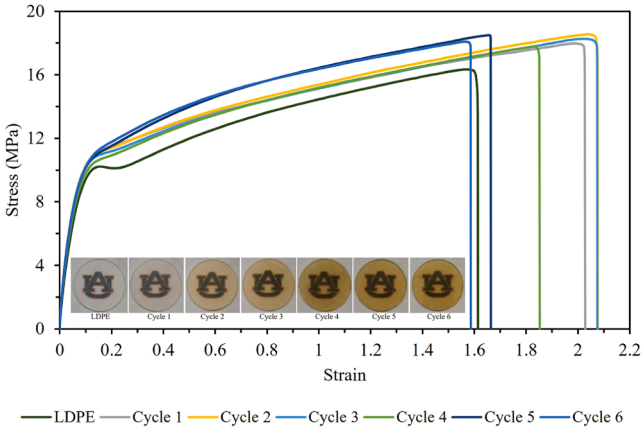

Fig. 2. Stress-strain curves of LDPE and the reprocessed blend.

suggests a potential concern for color-sensitive applications.

The tensile strength and secant modulus at 5 % strain are exhibited in Fig. 3. Both tensile strength and secant modulus at 5 % strain exhibited remarkable stability throughout the reprocessing cycles, which were all greater than that of neat LDPE (16.4 MPa and 135 MPa). This consistency illustrates the reprocessed blend's robustness against external stress. The esterification reaction between LLDPE-g-MA and EVOH likely played a major role in contributing to this trend. It helped establish a pathway for stress transfer between LDPE and EVOH, reducing stress concentration. The result suggests the thermomechanical processes applied during reprocessing did not substantially alter the blend's tensile strength and stiffness.

The tensile energy to break and elongation at break are shown in Fig. 4. The tensile energy to break increased from 21.1 MJ/m^3 (LDPE) to 29.7 MJ/m^3 in Cycle 1 and stayed stable up to Cycle 3, indicating the reprocessed blend had a good energy absorption capacity. This is attributed to a good compatibility of the reprocessed blend in early reprocessing stage. However, the tensile energy to break started to decrease from Cycle 4, and the value reached the same level as neat LDPE at Cycle 5 and 6. A similar trend was observed for the elongation at break. The declines in tensile energy at break and elongation at break suggest a reduced capacity of the reprocessed blend to undergo plastic deformation prior to fracture. As the reaction between LLDPE-g-MA and EVOH intensified, EVOH gelling occurred, leading to phase separation, and subsequently weakening the connection between LDPE and EVOH. This gelling was verified through morphological observations.

The EWF measurement results are shown in Fig. 5. Typical load-displacement curves for LDPE and the blend in Cycle 1, as a function of varying ligament lengths ranging from 4 to 8 mm, are shown in Fig. 5 (a) and (c). The specific total work of fracture (w_f) was calculated by normalizing the area under the load-displacement curves to the specimen thickness. The plots of w_f against ligament length for LDPE and the blend in Cycle 1 are shown in Fig. 5(b) and (d). A linear regression analysis was performed on the plots of w_f against ligament length, from which the intercept and the slope, corresponding to w_e and βw_p, were determined and summarized in Table 1. The same analyses were applied to the reprocessed blend from Cycle 2 to Cycle 6 to acquire data. Excellent geometrical self-similarity was observed in all the load-displacement curves across different ligament lengths for both LDPE and the reprocessed blend. This suggests that variations in ligament length had no significant influence on the fracture behavior, thereby confirming the validity of using the EWF method [35,37]. Both LDPE and the reprocessed blend showed ductile behavior, demonstrated by their capacity for large plastic deformation.

There was a noticeable enhancement in the EWF value from 17.0 kJ/m^2 for LDPE to 18.5 kJ/m^2 for the blend in Cycle 1, as shown in Table 1, indicating that the inclusion of EVOH and LLDPE-g-MA distinctly improved LDPE's toughness. This enhancement can be attributed to LLDPE-g-MA, which served as a compatibilizer and improved the interfacial adhesion between LDPE and EVOH phases, leading to a greater energy absorption capability before fracture [31]. The EWF value for the reprocessed blend initially increased as the number of reprocessing cycles increased, reaching a peak of 26.4 kJ/m^2 in Cycle 3, followed by subsequent declines. The EWF value dropped to 20.1 kJ/m^2 in Cycle 5 and further diminished to 17.7 kJ/m^2 in Cycle 6, closely resembling the toughness of the original LDPE matrix. These observations suggest that while blending initially enhanced toughness due to the compatibilization effect, repeated thermomechanical reprocessing adversely affected the toughness of the blend, likely owing to the gelling of EVOH.

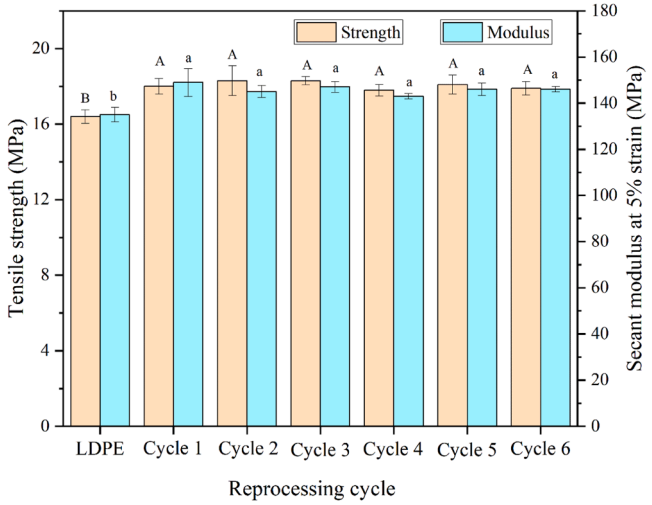

Fig. 3. Tensile strengths and secant moduli of LDPE and the reprocessed blend.

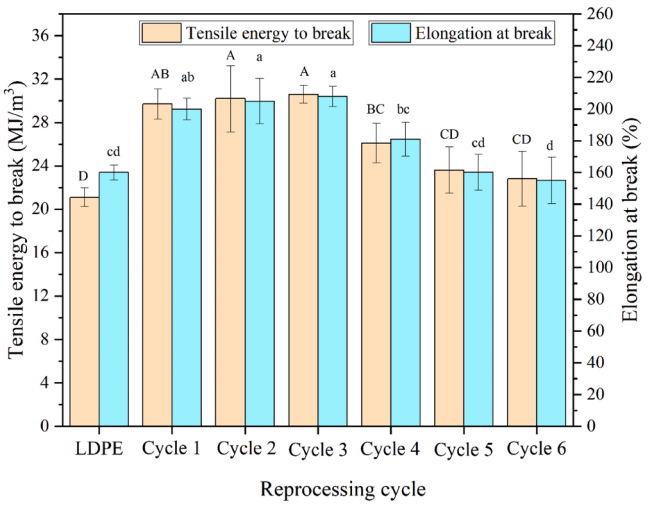

Fig. 4. Tensile energies to break and elongations at bleak of LDPE and the reprocessed blend.

For the neat LDPE sample, the βw_p value was 14.0 MJ/m^3, reflecting the material's inherent resistance to external deformation during fracture propagation. Upon reprocessing the blend in Cycle 1, the βw_p value increased slightly to 15.0 MJ/m^3. The slight increase in βw_p value could be attributed to enhanced intermolecular interactions and increased potential for energy dissipation, resulting from the reaction between LLDPE-g-MA and EVOH. However, as the blend underwent successive thermomechanical reprocessing cycles, a trend of decreasing βw_p values was observed. After reprocessing in Cycle 6, the βw_p value of the blend decreased to 11.5 MJ/m^3. This suggests that increased thermomechanical reprocessing diminished the blend's ability to absorb and dissipate energy through non-essential plastic deformation processes. Such a decline could result from changes in the phase morphology or potential degradation of EVOH, leading to less effective stress transfer and energy absorption. The coefficient of determination (R^2) values consistently maintained commendable levels across various samples, ranging between 0.93 and 0.96. This high range of R^2 values affirmed the validity of the EWF theory and indicated that the test results obtained through the EWF method were reliable.

The tensile and EWF testing results consistently demonstrate that the mechanical performance of the reprocessed blend is maintained for up to four reprocessing cycles without significant decrease.

3.2. Morphologies

The morphologies of the cross-sections of LDPE and the reprocessed blend are shown in Fig. 6. The SEM image revealed that the cross-section of the neat LDPE matrix had a homogeneous and relatively smooth morphology without any apparent voids. Some scratch marks observed

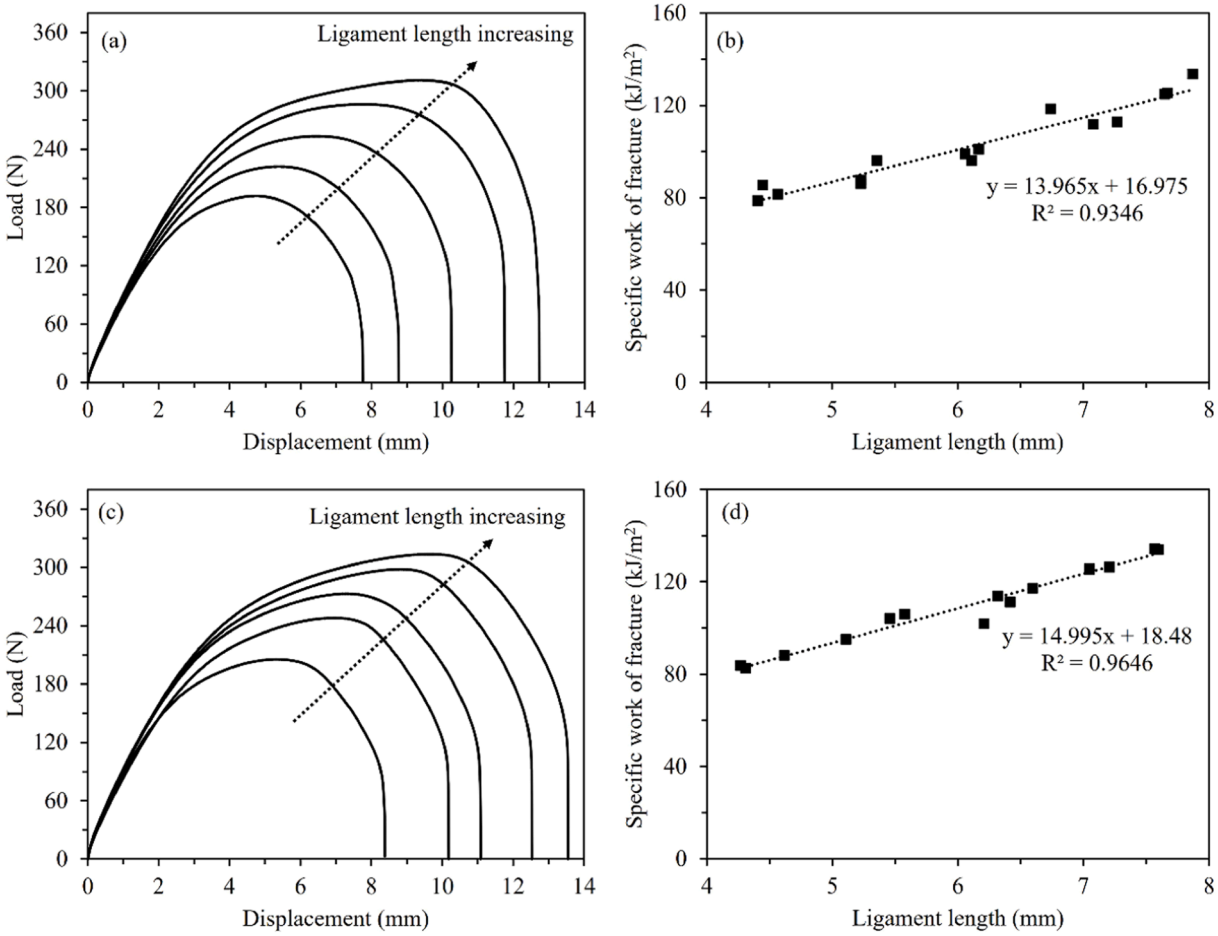

Fig. 5. Load-displacement curves of the DENT samples: (a) LDPE and (c) the reprocessed blend in Cycle 1, and the plots of total specific work of fracture versus ligament lengths: (b) LDPE and (d) the blend in Cycle 1.

Table 1
Specific EWF and non-EWF for LDPE and the reprocessed blend.

Sample name	EWF (w_e, kJ/m^2)	Non-EWF (βw_p, MJ/m^3)	Coefficient of determination (R^2)
LDPE	17.0	14.0	0.93
Cycle 1	18.5	15.0	0.96
Cycle 2	23.1	14.3	0.94
Cycle 3	26.4	13.1	0.94
Cycle 4	25.3	13.1	0.96
Cycle 5	20.1	12.3	0.96
Cycle 6	17.7	11.5	0.96

were caused by razor blade cutting during the specimen preparation process. The morphology of the blend in Cycle 1 displayed increased heterogeneity as the EVOH phase dispersed in the LDPE matrix [27]. Whereas the dispersion of the EVOH phase was relatively uniform and fine, benefiting from the interaction between LLDPE-g-MA and EVOH, which decreased interfacial tension and enhanced compatibility. [31]. This is also evidenced by the increased strength and toughness observed in mechanical tests. A few small holes, likely resulting from the removal of EVOH particles during sample preparation, were noted in the blend. This removal may have occurred when the sample was subjected to the pulling force from the razor blade.

With an increase in the number of reprocessing cycles, there was an improvement in the level of interaction between LLDPE-g-MA and EVOH. This improvement can be attributed to the formation of more ester linkages between LLDPE-g-MA and EVOH, which in turn caused the gelling of EVOH, thereby leading to an increase in rigidity. The gelling of EVOH particles was evidenced by the deformation of the LDPE matrix formed during sample preparation, as depicted in the SEM image of the cross-section of the reprocessed blend in Cycle 4. Upon the application of external force to the reprocessed blend, the gelling of EVOH particles made them less effective in absorbing and transferring stress. Consequently, the energy was primarily dissipated through deformation and crack propagation within the LDPE matrix. This led to more voids and weakened interphase interactions within the reprocessed blend, as verified by the decline in mechanical properties. Simultaneously, with ongoing cross-linking between LLDPE-g-MA and EVOH, the mobility of EVOH chains and the dispersion of EVOH domains became restricted during melt compounding. This resulted in agglomeration of the EVOH phase, leading to increased phase separation and, subsequently, a decrease in compatibility. After five cycles of reprocessing, a dramatic distortion in the LDPE matrix occurred caused by the dragging of the dispersed EVOH particles during sample preparation as a result of increased rigidity of EVOH after gelling.

The high-magnification images of the blend from Cycle 2 and Cycle 5 (Fig. 7) clearly demonstrate the morphology change, highlighting the morphological transition of dispersed EVOH particles from small to larger sizes. The morphology analysis suggests that while the compatibilization effect of LLDPE-g-MA enhanced the blend's performance in early stages of reprocessing, the gelling of EVOH adversely affected it in the latter two cycles of reprocessing.

3.3. FTIR spectra

The FTIR spectra of LDPE, LLDPE-g-MA, EVOH, and the reprocessed

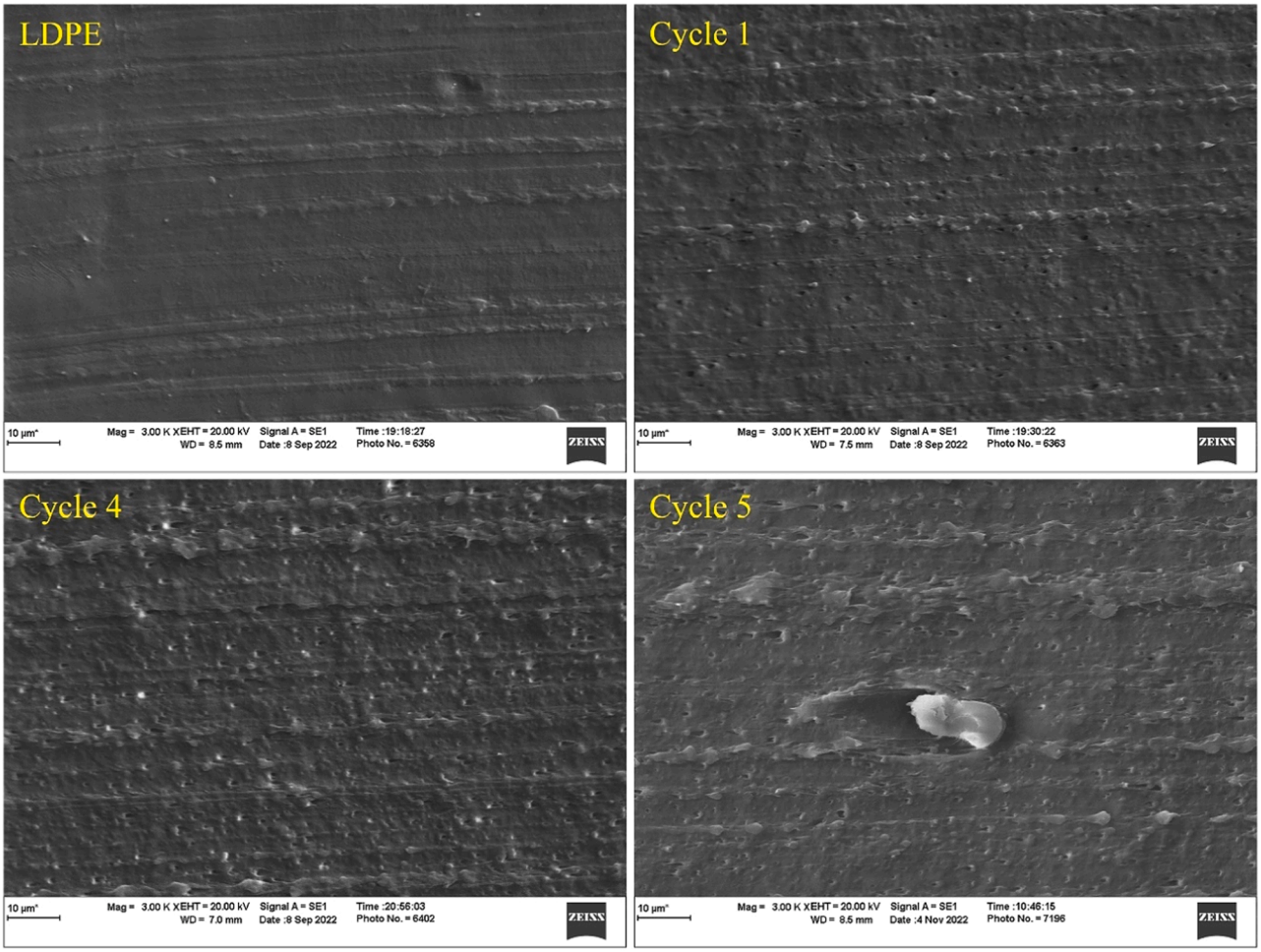

Fig. 6. SEM images of the cross-sections of LDPE and the reprocessed blend in Cycle 1, Cycle 4, and Cycle 5.

blend are shown in Fig. 8. The FTIR spectra of LDPE, LLDPE-g-MA, and EVOH each showed distinct absorption band characteristics of their respective chemical structures. In the FTIR spectrum of LDPE, the absorption bands at 2916 cm^{-1} and 2848 cm^{-1} correspond to asymmetric and symmetric CH_2 stretching vibrations, respectively, while the bands at 1463 cm^{-1} and 1419 cm^{-1} represent CH_2 bending vibrations [54]. The absorption bands at 3394 cm^{-1}, 3187 cm^{-1}, and 1645 cm^{-1} are associated with the amine group, originating from the commonly used hindered amine light stabilizer, aligning with the findings in Gulmine et al.'s work [55]. The absorption band at 1378 cm^{-1} corresponds to symmetric CH_3 bending vibrations [54,56]. The bands at 1301 cm^{-1} and 1262 cm^{-1} are attributed to C—H wagging vibrations, and the band at 1119 cm^{-1} represents a C—H twisting vibration [55]. The absorption bands at 816 cm^{-1}, 804 cm^{-1}, and 719 cm^{-1} are allocated to C—H out-of-plane bending vibrations [54].

The dominant absorption bands in the LLDPE-g-MA FTIR spectrum align with those of LDPE, confirming the presence of the PE backbone in LLDPE-g-MA. Moreover, a minor absorption band at 1792 cm^{-1}, seen in the enlarged insert, indicates the presence of a maleic anhydride graft, corresponding to C═O stretching vibrations [57,58]. In the EVOH spectrum, the stretching vibration absorption bands were observed at 3298 cm^{-1} for O—H, 2918 cm^{-1} for asymmetric C—H, and 2852 cm^{-1} for symmetric C—H. The bending vibration absorption bands appeared at 1455 cm^{-1} for asymmetric C—H and 1326 cm^{-1} for symmetric C—H [49,59,60]. The broad band at 1083 cm^{-1} in the EVOH spectrum corresponds to C—O stretching vibrations, which is characteristic of the alcohol units in EVOH [61].

The spectrum of the blend in Cycle 1 is similar to that of LDPE. From Cycle 2 through Cycle 4, there is a gradual decrease in the intensities at 3394 cm^{-1}, 3187 cm^{-1}, and 1645 cm^{-1} in the reprocessed blend when compared to the blend in Cycle 1. The reason for the reduced band intensities could be the scavenging of the light stabilizer due to thermo-oxidative degradation [55]. The band area ratios for the potential light stabilizer against the typical CH_2 stretching vibrations are presented in Table 2. The gradually reduced ratios from Cycle 1 to Cycle 4 imply a continuous reduction of the light stabilizer content. As the reprocessing cycles progressed to Cycle 5, the absorption bands at 3394 cm^{-1}, 3187 cm^{-1}, and 1645 cm^{-1} became undetectable, indicating the almost complete consumption of the light stabilizer. In the reprocessed blend from Cycle 5 and 6, a small new absorption band at 1720 cm^{-1} emerged, as found in the enlarged insert. This band could imply 1) an increase in the number of ester linkages (C═O) due to an intensified reaction between LLDPE-g-MA and EVOH [62], and/or 2) the formation of a small amount of C═O stretching vibrations caused by thermo-oxidative degradation in the presence of air [63]. The FTIR spectroscopy results confirmed the reaction between LLDPE-g-MA and EVOH and indicated the consumption of light stabilizer as the number of reprocessing cycles increased.

3.4. Thermal properties

Melting curves of LDPE, LLDPE-g-MA, EVOH, and the reprocessed blend are provided in Fig. 9. The melting points of LDPE and EVOH are 114 °C and 179 °C, respectively. LLDPE-g-MA had two melting peaks, with the main one at 121 °C and a small, broad one at a lower temperature, representing the melting peaks of PE whose crystalline

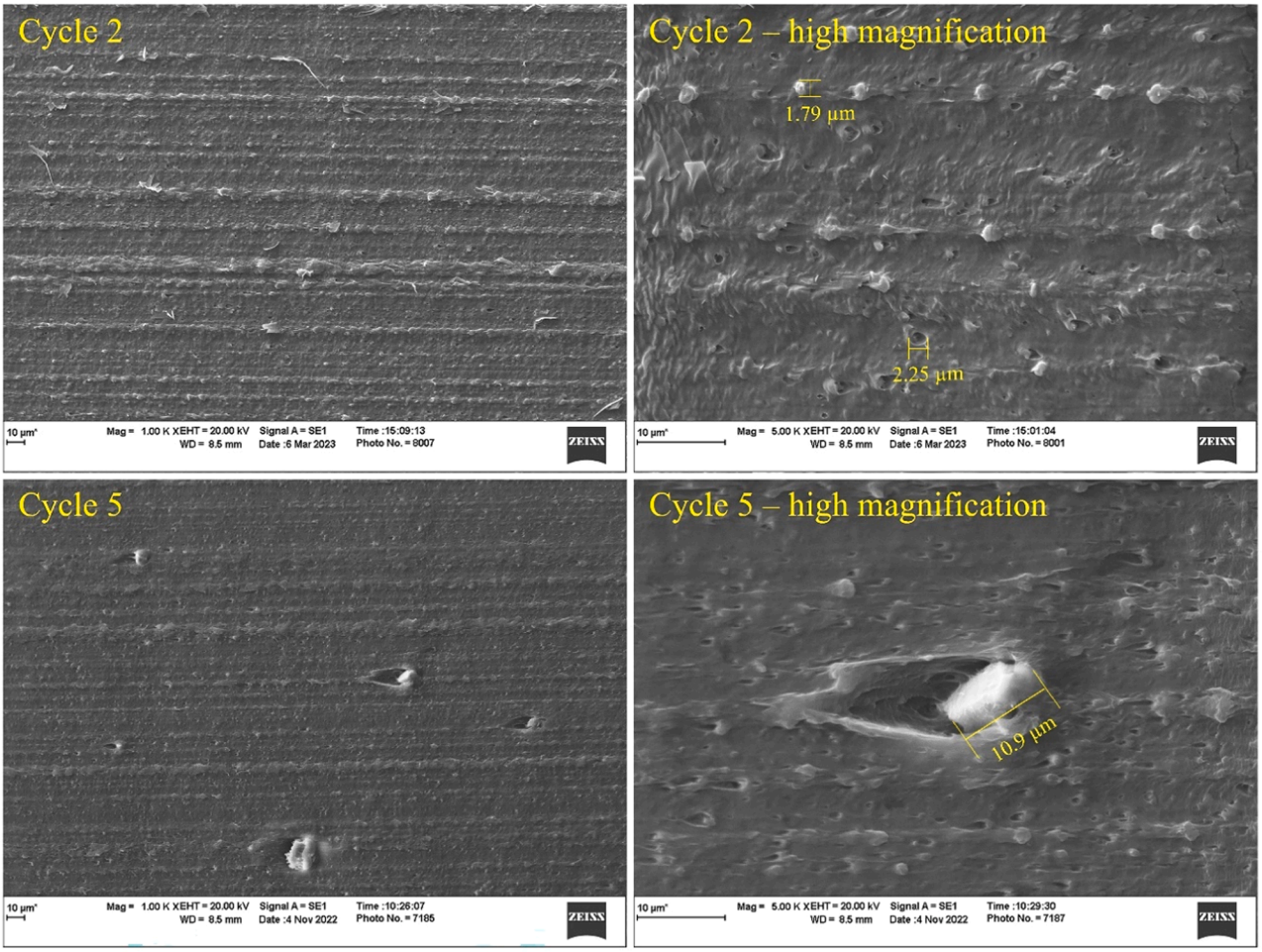

Fig. 7. High-magnification SEM images of the cross-sections of the reprocessed blend in Cycle 2 and Cycle 5.

structures were disrupted by the grafting of the maleic anhydride groups [64]. In Cycle 1 of the blend, the melting peaks of LDPE and LLDPE-g-MA merged, exhibiting a melting point of 113 °C. This melting point is comparable to that of LDPE, suggesting that LDPE played a dominant role in influencing the melting behavior of the PE component [65]. As the number of reprocessing cycles increased, the merged melting point of LDPE and LLDPE-g-MA in the reprocessed blend remained consistent, indicating negligible change in the melting behavior of these components when subjected to thermomechanical reprocessing for up to six cycles. On the contrary, the melting point of EVOH decreased to 173 °C in the blend of Cycle 1, due to the interaction between LLDPE-g-MA and EVOH, which disrupted the orderly crystalline regions of EVOH, making them less thermally stable and thereby lowering the temperature required to melt these regions [31]. The melting point of EVOH further decreased with an increase in reprocessing cycles, indicating a higher level of interactions between LLDPE-g-MA and EVOH, which in turn led to more disrupted crystalline regions.

The degrees of crystallinity for LDPE, LLDPE-g-MA, and EVOH as a function of thermomechanical reprocessing cycles are plotted in Fig. 10. The degrees of crystallinity for neat LDPE, LLDPE-g-MA, and EVOH were determined to be 26.3 %, 21.0 %, and 30.8 %, respectively. Since the melting peaks of LDPE and LLDPE-g-MA were primarily contributed by the PE content and were merged, the degrees of crystallinity for LDPE and LLDPE-g-MA were evaluated together and are labeled as "LDPE + LLDPE-g-MA" in Fig. 10. In the blend of Cycle 1, the degree of crystallinity for the LDPE + LLDPE-g-MA was 25.6 %, and this value remained stable for up to six cycles. However, for the blend in Cycle 1, the degree of crystallinity for EVOH was 12.1 %, significantly lower than that of neat EVOH. This reduction is attributed to the esterification reaction between LLDPE-g-MA and EVOH, as interpreted in its melting behavior, restricting the EVOH chains' mobility to rearrange into an orderly crystalline structure. As the number of reprocessing cycles increased, the degree of crystallinity for EVOH in the reprocessed blend progressively diminished, falling to 5.6 % in Cycle 6. The gradually reduced degree of crystallinity for EVOH, with an increase in reprocessing cycles further confirms the formation of less orderly crystalline regions. This decreased trend highlights the significant impact of thermomechanical reprocessing on the degree of crystallinity for EVOH.

Crystallization curves of LDPE, LLDPE-g-MA, EVOH, and the reprocessed blend are displayed in Fig. 11. The crystallization peak temperatures of LDPE, LLDPE-g-MA, and EVOH were 97 °C, 105 °C, and 156 °C, respectively. Similar to their melting behaviors, the crystallization peaks of LDPE and LLDPE-g-MA merged in the reprocessed blend in Cycle 1, exhibiting a crystallization peak temperature at 100 °C. This merged crystallization peak temperature remained comparable from Cycle 1 to Cycle 6, suggesting that LDPE and LLDPE-g-MA can withstand at least six reprocessing cycles without significant changes in their crystallization properties. Conversely, EVOH in the blend of Cycle 1 had a crystallization peak temperature of 148 °C, remarkably lower than that of neat EVOH. The crystallization peak temperature of EVOH in the reprocessed blend progressively decreased to 143 °C by Cycle 6, displaying a similar change to that seen in its melting behavior. The decline in crystallization temperatures is also attributed to the constraining effect induced by the cross-linking between LLDPE-g-MA and EVOH, which hindered the crystallization process of EVOH [31,66].

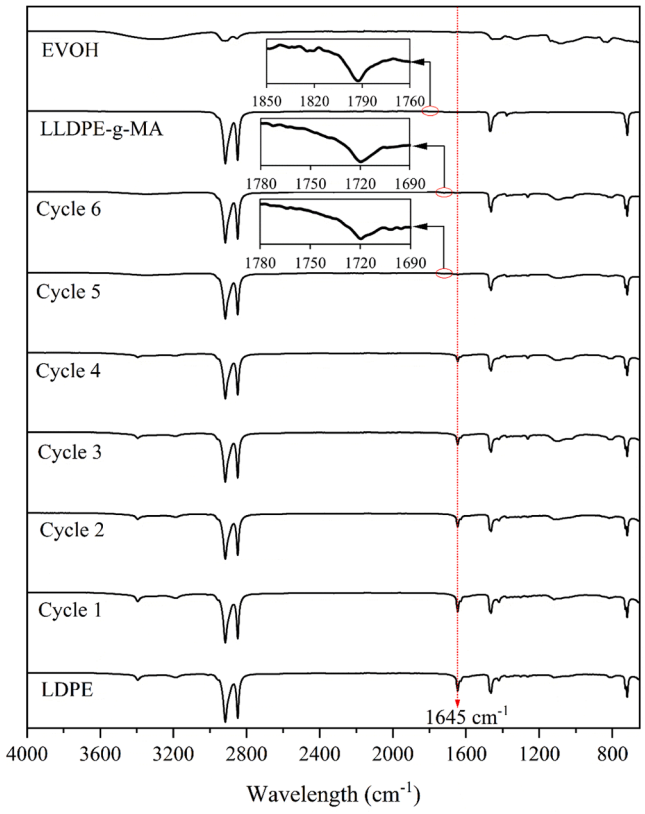

Fig. 8. FTIR spectra of LDPE, LLDPE-g-MA, EVOH, and the reprocessed blend.

Table 2
FTIR spectrum band area ratios of LDPE and the reprocessed blend.

Sample name	Relative band intensities of the light stabilizer against typical bands for CH_2 stretching vibrations (%)		
	$I_{3394}/(I_{2916}+I_{2848})$	$I_{3187}/(I_{2916}+I_{2848})$	$I_{1645}/(I_{2916}+I_{2848})$
LDPE	8.40 ± 0.75	4.88 ± 0.19	13.1 ± 0.55
Cycle 1	8.19 ± 0.54	4.81 ± 0.15	12.4 ± 1.37
Cycle 2	6.53 ± 0.29	3.01 ± 0.33	9.59 ± 0.67
Cycle 3	5.87 ± 0.49	2.36 ± 0.41	7.67 ± 0.86
Cycle 4	4.90 ± 0.90	1.36 ± 0.09	6.32 ± 0.67

*The values after "±" symbol refer to the standard deviations.

The DSC results indicate that while LDPE and LLDPE-g-MA can withstand at least six reprocessing cycles without significant change in thermal properties, EVOH in the blend is more susceptible to thermo-mechanical reprocessing. The DSC results also imply the importance of considering the potential degradation of individual components in blend when assessing their recyclability and reusability as a polymer blend.

3.5. Rheological properties

The storage modulus (G') and loss modulus (G'') as functions of frequency are depicted in Fig. 12. In Cycle 1, the blend exhibited higher G' and G'' values compared to neat LDPE, likely arising from the improved stiffness induced by the incorporation of the inherently rigid EVOH phase and the restricted chain mobility due to the in-situ reaction established by LLDPE-g-MA. However, a slight decline in both G' and G'' was observed in Cycle 2, probably due to enhanced thermo-oxidative and shear-induced degradation under the reprocessing conditions [67]. An exception was found in Cycle 3, where both G' and G'' were higher than their corresponding values in Cycle 2 but remained below those in Cycle 1. Repeated thermal treatment facilitated the

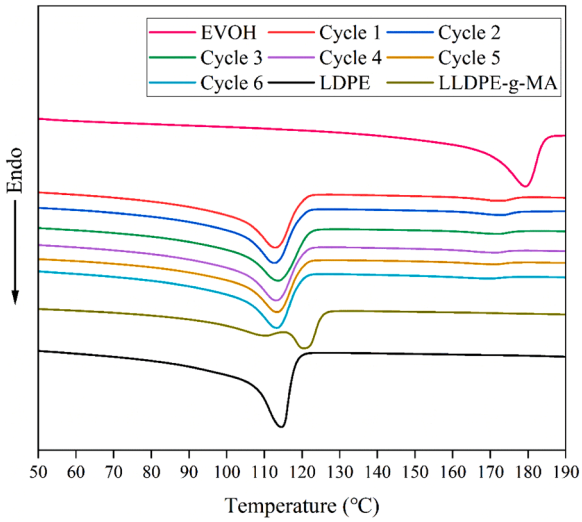

Fig. 9. Melting curves of LDPE, LLDPE-g-MA, EVOH, and the reprocessed blend.

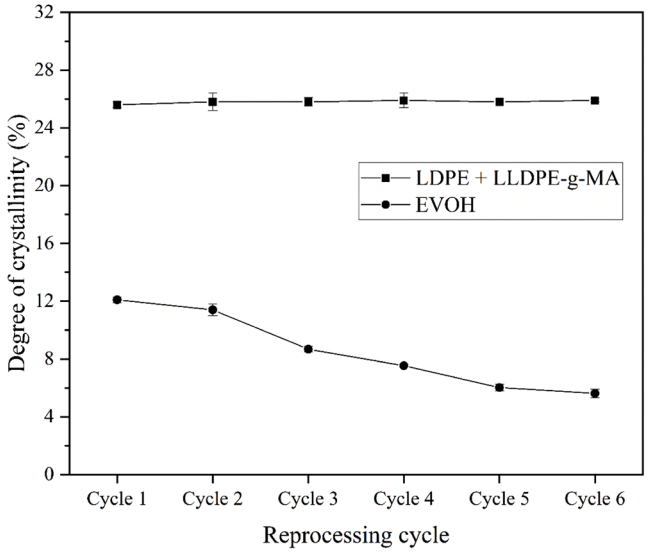

Fig. 10. Degree of crystallinity of LDPE, LLDPE-g-MA, and EVOH in the reprocessed blend.

cross-linking between LLDPE-g-MA and EVOH, leading to the increased moduli in Cycle 3. With a further increase in reprocessing cycles, gelled EVOH particles were formed due to the increased cross-linking, leading to a subsequent reduction in the compatibility of the reprocessed blend. The low compatibility resulted in decreased interfacial adhesion, ultimately causing a slight reduction in viscoelastic properties as interfacial slip occurred during the rheological test [68]. Overall, thermomechanical reprocessing appeared to have a minimal impact on the viscoelastic behavior of the reprocessed blend, as evidenced by the low-amplitude changes observed in both G' and G'' values.

The complex viscosity (η^*) of LDPE and the reprocessed blend was examined as a function of frequency and is presented in Fig. 13. The η^* of the reprocessed blend followed similar trends as those noted for G' and G''. The flow behavior of the reprocessed blend in each cycle was consistent with shear-thinning tendency and followed Cross-like rheological behavior, the mathematical expression of the Cross model is as below [69]:

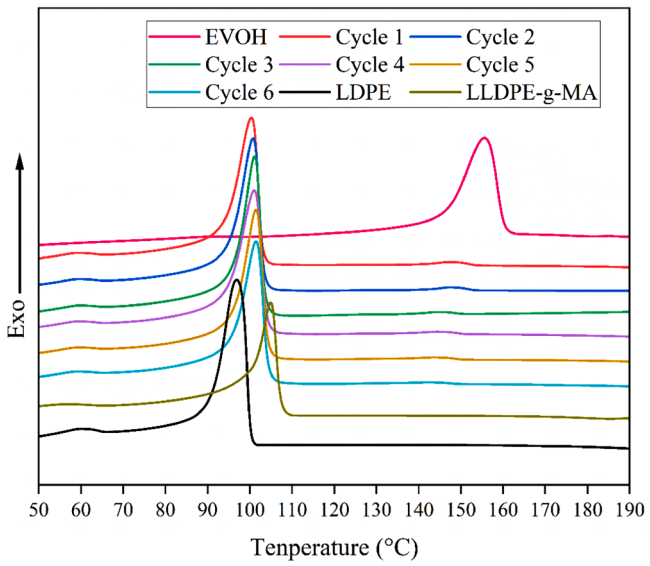

Fig. 11. Crystallization curves of LDPE, LLDPE-g-MA, EVOH, and the reprocessed blend.

$$\eta = \frac{\eta_0}{(1+\lambda\omega)^{1-n}}$$

where λ is the characteristic time and n is the flow index. The fitted flow indexes tended to increase with respect to reprocessing cycles (Table 3), indicating reduced shear thinning as the increased cross-linking. The fitted zero-shear viscosity (η_0) was greatly impacted and prone to grow substantially with respect to the reprocessing cycles (Table 3). As a result, the increased viscosity and reduced shear-thinning behavior of the polymeric melt due to the increasing number of reprocessing cycles could potentially result in challenging conditions for subsequent reprocessing.

The van Gurp Palmen (vGP) plot provides information about MW, polydispersity, and morphology. For polymer blends with different MW components, it is known that the vGP plot will display multiple minimums in the phase angle (δ) [70–72]. Moreover, a reduction in the primary phase angle minimums (δ_{min}) implies an increase in MW [73]. The vGP plots of LDPE and the reprocessed blend are provided in Fig. 14 (a).

The vGP plots were relatively consistent among all the reprocessing cycles in terms of the minimum phase angle. There was a slight increase in the primary minimum phase angle from Cycle 1 to 6, but more interestingly, the complex modulus (G^*) at the minimum phase angle was more greatly impacted. The G^* was observed to decrease over the reprocessing cycles due to decreased stress transfer between LDPE and EVOH caused by EVOH gelling, which indicates an overall drop in

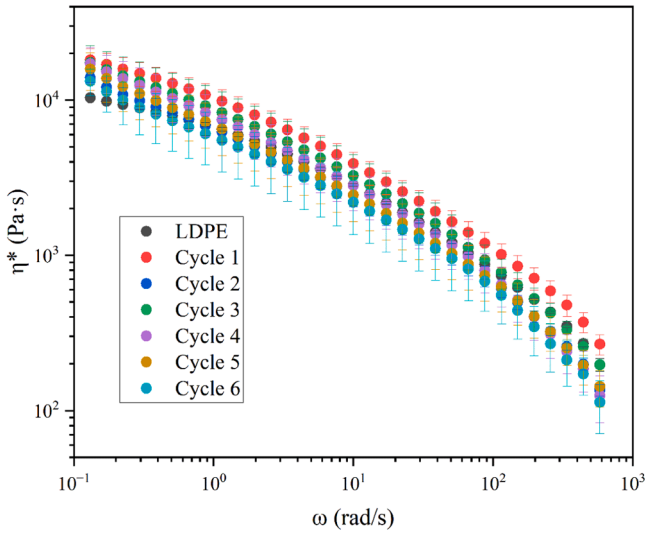

Fig. 13. Complex viscosity curves of LDPE and the reprocessed blend.

Table 3
Fitted Cross rheological model parameters of LDPE and the reprocessed blend.

Sample name	Zero-shear viscosity (η_0, Pa s)	Characteristic time (λ, s)	Power-law index (n)	Coefficient of determination (R^2)
LDPE	11,038	1.71	0.514	>0.99
Cycle 1	21,192	3.39	0.515	>0.99
Cycle 2	21,978	15.73	0.561	>0.99
Cycle 3	23,234	7.56	0.539	>0.99
Cycle 4	26,601	12.90	0.532	>0.99
Cycle 5	32,703	32.41	0.549	>0.99
Cycle 6	37,871	91.19	0.578	>0.99

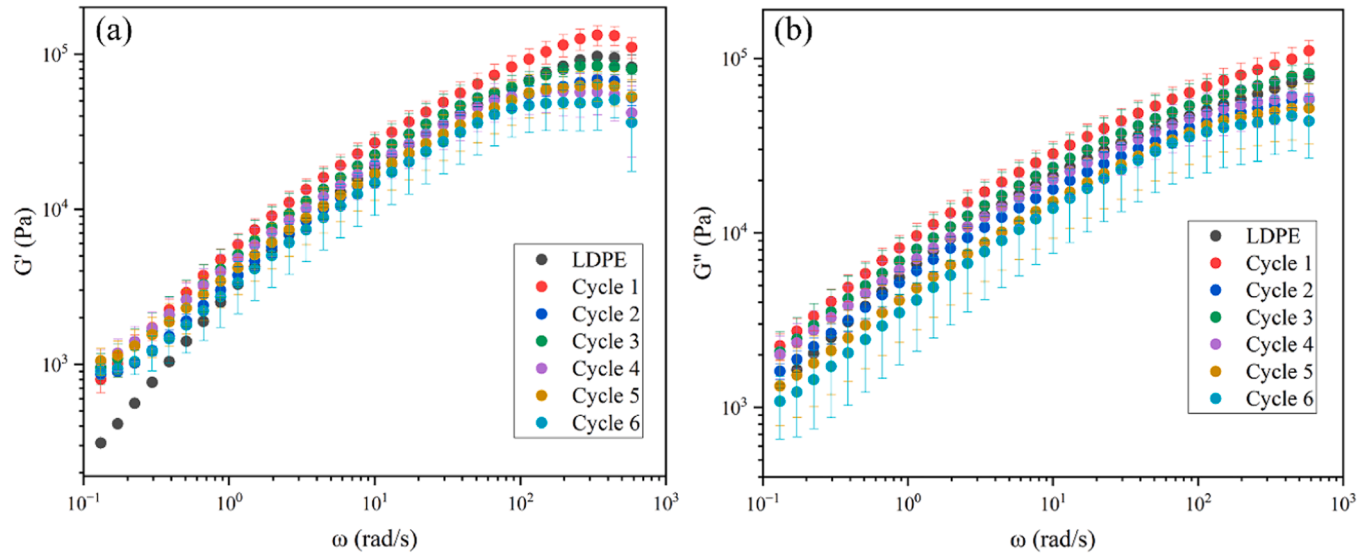

Fig. 12. Storage modulus (a) and loss modulus (b) vs frequency plots of LDPE and the reprocessed blend.

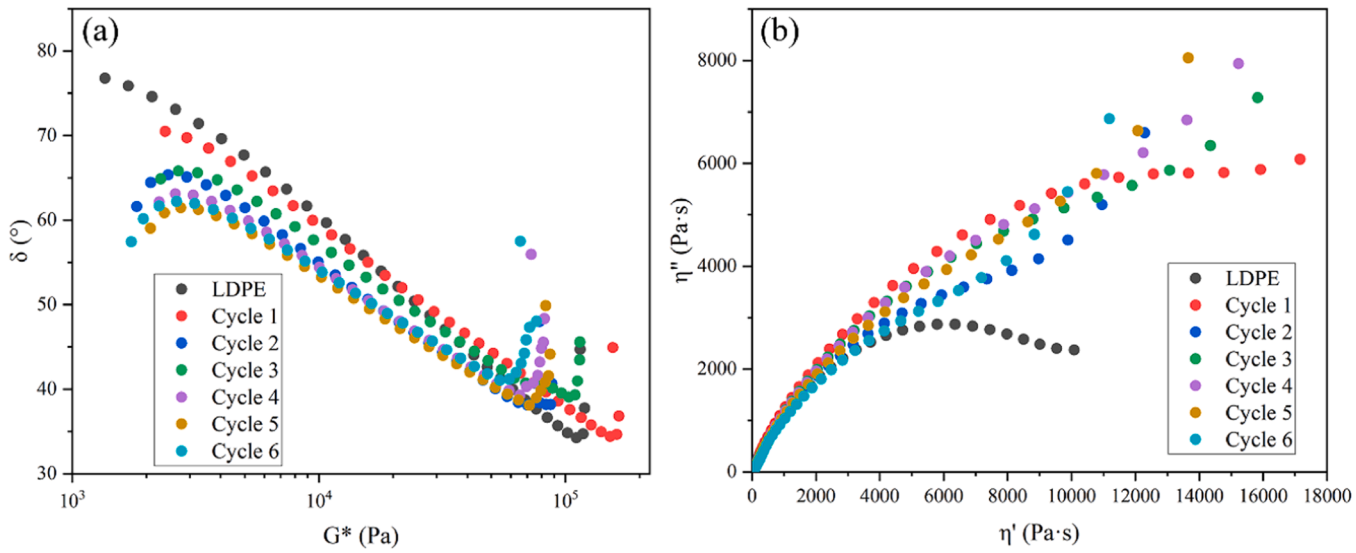

Fig. 14. Van Gurp Palmen (vGP) plots (a) and Cole-Cole plots (b) of LDPE and the reprocessed blend.

reprocessed blend's resistance to deformation during shear. Additionally, compared to LDPE, an apparent hesitation was noted for the reprocessed blend at similar G^* and phase angle value. This hesitation likely indicates a secondary minimum outside of the probed rheological range of the blend, which could arise from the secondary and ternary components within the blend or a significant change in molecular architecture induced by cross-linked structures. In either case, this hesitation was not dramatically changed with the increasing reprocessing cycles, though broadening the approach to the terminal flow plateau ($\delta \rightarrow 90°$), suggesting a slightly broadened MW distribution in the reprocessed blend.

The Cole-Cole plot provides detailed information about several rheological factors, such as polymer blend miscibility, mean relaxation time, and overall relaxation processes [74,75]. Fig. 14(b) shows Cole-Cole plots for LDPE and the reprocessed blend. A near-ideal Maxwellian-like behavior, indicated by a semicircular arc, was observed in LDPE. The reprocessed blend exhibited several different behaviors compared to LDPE. The initial consequence of blending LDPE, EVOH, and LLDPE-g-MA is shown in Cycle 1, where a dramatic increase in the arc of η' versus η'' was observed. The increase in arc radius implies a longer and more complex relaxation process, which is induced by the enhanced intermolecular interaction through cross-linking [76]. Moreover, the absence of a significant tail at high η' in this semicircular arc indicates the blend's miscibility in Cycle 1, verifying the compatibilization effect of LLDPE-g-MA. From Cycle 2 to 6, 'tailing' occurred at high η', indicating a secondary relaxation process. This secondary relaxation process could result from the broader MW distributions formed due to cross-linking or thermo-oxidative degradation. This analysis indicates that a fundamental change in the relaxation behavior of the reprocessed blend was introduced by thermomechanical reprocessing.

Rheological time sweep plots of LDPE and the reprocessed blend are provided in Fig. 15. The storage modulus values as a function of time were measured to evaluate the thermal stability of LDPE and the reprocessed blend. The storage modulus of LDPE remained constant as time increased to 30 min, which can be attributed to its low susceptibility to thermal treatment. While the storage modulus of the reprocessed blend increased as time progressed, this can be explained by the improved phase interaction resulting from the reactive interaction between LLDPE-g-MA and EVOH, which made the blend more rigid. Additionally, as the number of reprocessing cycles increased, the storage modulus of the reprocessed blend decreased. This decrease is attributed to reduced interfacial adhesion caused by increased phase separation, as

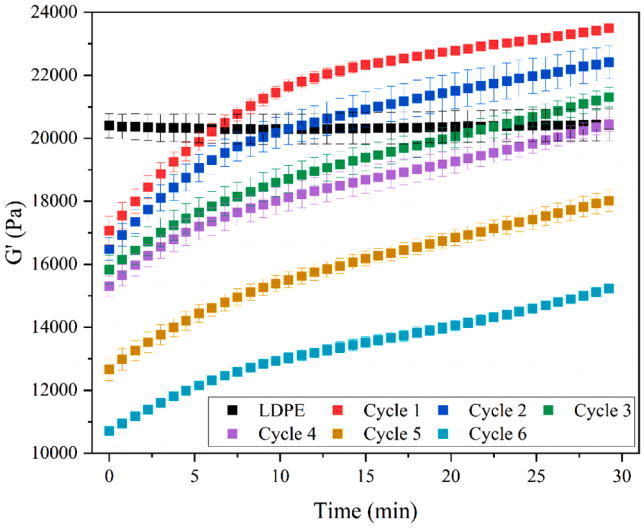

Fig. 15. Time sweep plots of LDPE and the reprocessed blend.

the continuously increased cross-linking of the EVOH phase resulted in larger particle sizes. This, in turn, can lead to inefficient stress transfer across the interface. A remarkable increase in the magnitude of the decrease in storage modulus was observed starting from Cycle 5, implying a distinct transition in the properties of the reprocessed blend.

4. Conclusion

The recycling and reutilization of MPP has garnered significant attention owing to its rapidly expanding market. Polymer blending is expected to be a promising strategy since it eliminates the need to separate the complex structure of MPP. Nevertheless, the underlying polymer degradation induced by the thermomechanical reprocessing in melt blending, and its subsequent influence on the reprocessed MPP's performance, remain unclear. In this study, the impact of thermomechanical reprocessing on the properties of LDPE-based MPP with EVOH as a barrier layer was investigated. The LDPE/LLDPE-g-MA/EVOH blend was subjected to six cycles of reprocessing, including thermal compounding, mechanical grinding, and injection molding. The mechanical performance, morphological features, chemical composition, thermal behavior, and rheological properties were characterized

after each reprocessing cycle.

The tensile strength and modulus were relatively consistent for all six cycles, while a marked decrease in elongation at break was observed starting from Cycle 4. A noticeable darkening in color was observed as the number of reprocessing cycles increased, primarily caused by thermo-oxidative degradation. As evaluated by the EWF characterization, the toughness of the blend decreased after four cycles of reprocessing. The morphology analysis revealed that the gelling of EVOH is the major reason for the reduction in the blend's mechanical performance. The FTIR spectroscopy results verified that the reactive interaction between LLDPE-g-MA and EVOH occurred during thermomechanical reprocessing and intensified with successive reprocessing cycles. The thermal properties of LDPE and LLDPE-g-MA within the reprocessed blend remained stable. However, the melting temperature, crystallization temperature, and degree of crystallinity of the EVOH decreased as the number of reprocessing cycles increased. The continuous reprocessing had a minor impact on rheological properties.

Reprocessing LDPE-based MPP through polymer blending can be an effective method for up to four cycles concerning the mechanical, thermal, and rheological behaviors of the reclaimed MPP material. Future research will investigate methods for extracting the EVOH composition susceptible to thermomechanical reprocessing before manufacturing the polymer blend.

CRediT authorship contribution statement

Ke Zhan: Writing – review & editing, Writing – original draft, Methodology, Investigation, Formal analysis, Data curation. **Daniel Meadows:** Writing – review & editing, Investigation, Formal analysis, Data curation. **Lindsay Levy:** Investigation, Data curation. **Raymond Hou:** Investigation, Data curation. **Tanmay Rahman:** Investigation, Data curation. **Virginia Davis:** Writing – review & editing. **Edward Davis:** Writing – review & editing, Project administration. **Bryan S. Beckingham:** Writing – review & editing. **Brian Via:** Writing – review & editing. **Thomas Elder:** Writing – review & editing. **Yucheng Peng:** Writing – review & editing, Supervision, Funding acquisition, Conceptualization.

Declaration of competing interest

The authors declare that they have no known competing financial interests or personal relationships that could have appeared to influence the work reported in this paper.

Data availability

Data will be made available on request.

Acknowledgments

This work was supported by the National Science Foundation (NSF-EFRI # 2132093). We acknowledge Berry Global Inc. for providing LDPE, LLDPE-g-MA, and EVOH pellets.

References

[1] X. Chen, N. Kroell, J. Wickel, A. Feil, Determining the composition of post-consumer flexible multilayer plastic packaging with near-infrared spectroscopy, Waste Manag. 123 (2021) 33–41.
[2] T. Anukiruthika, P. Sethupathy, A. Wilson, K. Kashampur, J.A. Moses, C. Anandharamakrishnan, Multilayer packaging: advances in preparation techniques and emerging food applications, Compr. Rev. Food Sci. Food Saf. 19 (3) (2020) 1156–1186.
[3] G. Cabrera, J. Li, A. Maazouz, K. Lamnawar, A journey from processing to recycling of multilayer waste films: a review of main challenges and prospects, Polymers 14 (12) (2022).
[4] D. Briassoulis, P. Tserotas, M. Hiskakis, Mechanical and degradation behaviour of multilayer barrier films, Polym. Degrad. Stab. 143 (2017) 214–230.
[5] T.W. Walker, N. Frelka, Z. Shen, A.K. Chew, J. Banick, S. Grey, M.S. Kim, J. A. Dumesic, R.C. Van Lehn, G.W. Huber, Recycling of multilayer plastic packaging materials by solvent-targeted recovery and precipitation, Sci. Adv. 6 (47) (2020) eaba7599.
[6] Z.O.G. Schyns, M.P. Shaver, Mechanical recycling of packaging plastics: a review, Macromol. Rapid Commun. 42 (3) (2021) 2000415.
[7] K. Ragaert, L. Delva, K. Van Geem, Mechanical and chemical recycling of solid plastic waste, Waste Manag. 69 (2017) 24–58.
[8] K.P. Pandey, U.R. Jha, J. Kushwaha, M. Priyadarsini, S.U. Meshram, A.S. Dhoble, Practical ways to recycle plastic: current status and future aspects, J. Mater. Cycles Waste Manag. 25 (3) (2023) 1249–1266.
[9] W. Camacho, S. Karlsson, Assessment of thermal and thermo-oxidative stability of multi-extruded recycled PP, HDPE and a blend thereof, Polym. Degrad. Stab. 78 (2) (2002) 385–391.
[10] G.W. Curtzwiler, M. Schweitzer, Y. Li, S. Jiang, K.L. Vorst, Mixed post-consumer recycled polyolefins as a property tuning material for virgin polypropylene, J. Clean. Prod. 239 (2019) 117978.
[11] I. Velghe, B. Buffel, V. Vandeginste, W. Thielemans, F. Desplentere, Review on the degradation of poly(lactic acid) during melt processing, Polymers 15 (9) (2023).
[12] A.A. Mendes, A.M. Cunha, C.A. Bernardo, Study of the degradation mechanisms of polyethylene during reprocessing, Polym. Degrad. Stab. 96 (6) (2011) 1125–1133.
[13] J. Stasiek, R. Malinowski, T. Ligor, B. Buszewski, GC/MS analysis of gaseous degradation products formed during extrusion blow molding process of PE films, Chem. Pap. 64 (5) (2010).
[14] K. Wang, F. Addiego, N. Bahlouli, S. Ahzi, Y. Rémond, V. Toniazzo, R. Muller, Analysis of thermomechanical reprocessing effects on polypropylene/ethylene octene copolymer blends, Polym. Degrad. Stab. 97 (8) (2012) 1475–1484.
[15] D. Lin, R. Li, Y. Liu, S. Qi, D. Wu, Clarifying the effect of moisture absorption and high-temperature thermal aging on structure and properties of polyimide film at molecular dynamic level, Polymer 214 (2021) 123251.
[16] E. Yousif, R. Haddad, Photodegradation and photostabilization of polymers, especially polystyrene: review, Springerplus 2 (1) (2013) 398.
[17] S. Saikrishnan, D. Jubinville, C. Tzoganakis, T.H. Mekonnen, Thermo-mechanical degradation of polypropylene (PP) and low-density polyethylene (LDPE) blends exposed to simulated recycling, Polym. Degrad. Stab. 182 (2020) 109390.
[18] H. Jin, J. Gonzalez-Gutierrez, P. Oblak, B. Zupančič, I. Emri, The effect of extensive mechanical recycling on the properties of low density polyethylene, Polym. Degrad. Stab. 97 (11) (2012) 2262–2272.
[19] J.M. Pérez, J.L. Vilas, J.M. Laza, S. Arnáiz, F. Mijangos, E. Bilbao, M. Rodríguez, L. M. León, Effect of reprocessing and accelerated ageing on thermal and mechanical polycarbonate properties, J. Mater. Process. Technol. 210 (5) (2010) 727–733.
[20] P. Sánchez, P. Remiro, J. Nazábal, Influence of reprocessing on the mechanical properties of a commercial polysulfone/polycarbonate blend, Polym. Eng. Sci. 32 (2004) 861–867.
[21] M.H. Martins, M.-A. De Paoli, Polypropylene compounding with post-consumer material: II. Reprocessing, Polym. Degrad. Stab. 78 (3) (2002) 491–495.
[22] P. Main, S. Petersmann, N. Wild, M. Feuchter, I. Duretek, M. Edeleva, P. Ragaert, L. Cardon, T. Lucyshyn, Impact of multiple reprocessing on properties of polyhydroxybutyrate and polypropylene, Polymers 15 (20) (2023).
[23] V. Lahtela, S. Silwal, T. Karki, Re-processing of multilayer plastic materials as a part of the recycling process: the features of processed multilayer materials, Polymers 12 (11) (2020).
[24] Z. Tartakowski, Recycling of packaging multilayer films: new materials for technical products, Resour., Conserv. Recycl. 55 (2) (2010) 167–170.
[25] C.I.K. Diop, J.-M. Lavoie, M.A. Huneault, Separation and reuse of multilayer food packaging in cellulose reinforced polyethylene composites, Waste Biomass Valoriz. 8 (1) (2016) 85–93.
[26] M.C. Mistretta, V. Titone, F.P. La Mantia, V. Pellitteri, L. Botta, Recycling of a multilayer barrier food packaging through the use of a nanofiller: effect of post-consumer plastic bag conditions, Polym. Test. 128 (2023) 108224.
[27] Y. Nasri, M.T. Benaniba, M. Bouquey, Elaboration and characterization of polymers used in flexible multilayer food packaging, Mater. Today 53 (2022) 91–95.
[28] K. Kaiser, M. Schmid, M. Schlummer, Recycling of polymer-based multilayer packaging: a review, Recycling 3 (1) (2017).
[29] K. Hamad, M. Kaseem, F. Deri, Effect of recycling on rheological and mechanical properties of poly(lactic acid)/polystyrene polymer blend, J. Mater. Sci. 46 (9) (2010) 3013–3019.
[30] C.-H. Huang, J.-S. Wu, C.-C. Huang, L.-S. Lin, Morphological, thermal, barrier and mechanical properties of LDPE/EVOH blends in extruded blown films, J. Polym. Res. 11 (1) (2004) 75–83.
[31] S.Y. Lee, S.C. Kim, Effect of compatibilizer on the crystallization, rheological, and tensile properties of LDPE/EVOH blends, J. Appl. Polym. Sci. 68 (8) (1998) 1245–1256.
[32] T. Hanae, P. Udo, S. Dominik, B. Roland, Recycling compatibility of EVOH barrier polymers in polyethylene-based packaging compositions, Inst. Cyclos-HTP GmbH (2022).
[33] G. Cabrera, M. Bouquey, R. Ibarra-Gomez, F. Lefort, S. Mani, T. Falher, Processing of polymer blends by twin-screw extrusion and reactive blending: a route towards the valorization of plastic food packaging waste, in: International Conference on Humans and Technology: A Holistic and Symbiotic Approach to Sustainable Development: Icht 2022, 2023.
[34] ASTM-882-12, Standard Test Method For Tensile Properties of Thin Plastic Sheeting, ASTM International ASTM, 2012. D20/D20.19.

[35] K. Saminathan, P. Selvakumar, N. Bhatnagar, Fracture studies of polypropylene/nanoclay composite. Part I: effect of loading rates on essential work of fracture, Polym. Test. 27 (3) (2008) 296–307.
[36] F.M. Peres, J.R. Tarpani, C.G. Schön, An assessment of essential work of fracture testing method applied to medium density polyethylene (MDPE), Eng. Fract. Mech. 105 (2013) 136–151.
[37] A.B. Martinez, J. Gamez-Perez, M. Sanchez-Soto, J.I. Velasco, O.O. Santana, M. Ll Maspoch, The essential work of fracture (EWF) method—Analyzing the post-yielding fracture mechanics of polymers, Eng. Fail. Anal. 16 (8) (2009) 2604–2617.
[38] M.M. Hossain, A.A. Kadam, C.-F. Lee, H.-J. Sue, D.M. Fiscus, Numerical modeling of essential work of fracture on ductile polymeric films, Eng. Fract. Mech. 212 (2019) 210–220.
[39] W. Yang, B.-H. Xie, W. Shi, Z.-M. Li, Z.-Y. Liu, J. Chen, M.-B. Yang, Essential work of fracture evaluation of fracture behavior of glass bead filled linear low-density polyethylene, J. Appl. Polym. Sci. 99 (4) (2006) 1781–1787.
[40] T. Bárány, T. Czigány, J. Karger-Kocsis, Application of the essential work of fracture (EWF) concept for polymers, related blends and composites: a review, Prog. Polym. Sci. 35 (10) (2010) 1257–1287.
[41] K.B. Broberg, Critical review of some theories in fracture mechanics, Int. J. Fract. Mech. 4 (1) (1968) 11–19.
[42] A.B. Martínez, A. Segovia, J. Gamez-Perez, M.L. Maspoch, Essential work of fracture analysis of the tearing of a ductile polymer film, Eng. Fract. Mech. 77 (14) (2010) 2654–2661.
[43] H.J. Kwon, P.Y.B. Jar, New energy partitioning approach to the measurement of plane-strain fracture toughness of high-density polyethylene based on the concept of essential work of fracture, Eng. Fract. Mech. 74 (16) (2007) 2471–2480.
[44] G. Gong, B.-H. Xie, W. Yang, Z.-M. Li, W.-q. Zhang, M.-B. Yang, Essential work of fracture (EWF) analysis for polypropylene grafted with maleic anhydride modified polypropylene/calcium carbonate composites, Polym. Test. 24 (4) (2005) 410–417.
[45] G. Gong, B.-H. Xie, W. Yang, Z.-M. Li, S.-M. Lai, M.-B. Yang, Plastic deformation behavior of polypropylene/calcium carbonate composites with and without maleic anhydride grafted polypropylene incorporated using the essential work of fracture method, Polym. Test. 25 (1) (2006) 98–106.
[46] D. Arencón, J.I. Velasco, V. Realinho, M. Antunes, M.L. Maspoch, Essential work of fracture analysis of glass microsphere-filled polypropylene and polypropylene/poly (ethylene terephthalate-co-isophthalate) blend-matrix composites, Polym. Test. 26 (6) (2007) 761–769.
[47] C. Ge, K. Lei, R. Aldi, Barrier, mechanical, and thermal properties of the three-layered co-extruded blown polyethylene/ethylene–vinyl alcohol/low density polyethylene film without tie layers, J. Thermoplast. Compos. Mater. 30 (6) (2015) 794–807.
[48] Y. Kong, J.N. Hay, The enthalpy of fusion and degree of crystallinity of polymers as measured by DSC, Eur. Polym. J. 39 (8) (2003) 1721–1727.
[49] A. Aragon-Gutierrez, E. Rosa, M. Gallur, D. Lopez, P. Hernandez-Munoz, R. Gavara, Melt-processed bioactive EVOH films incorporated with ferulic acid, Polymers 13 (1) (2020).
[50] F. Luzi, D. Puglia, F. Dominici, E. Fortunati, G. Giovanale, G.M. Balestra, L. Torre, Effect of gallic acid and umbelliferone on thermal, mechanical, antioxidant and antimicrobial properties of poly (vinyl alcohol-co-ethylene) films, Polym. Degrad. Stab. 152 (2018) 162–176.
[51] F. Luzi, L. Torre, D. Puglia, Antioxidant packaging films based on ethylene vinyl alcohol copolymer (EVOH) and caffeic acid, Molecules 25 (17) (2020) 3953.
[52] M. Roohani, Y. Habibi, N.M. Belgacem, G. Ebrahim, A.N. Karimi, A. Dufresne, Cellulose whiskers reinforced polyvinyl alcohol copolymers nanocomposites, Eur. Polym. J. 44 (8) (2008) 2489–2498.
[53] Y.C. Ching, T.M.S.U. Gunathilake, K.Y. Ching, C.H. Chuah, V. Sandu, R. Singh, N.-S. Liou, 18 - Effects of high temperature and ultraviolet radiation on polymer composites, in: M. Jawaid, M. Thariq, N. Saba (Eds.), Durability and Life Prediction in Biocomposites, Fibre-Reinforced Composites and Hybrid Composites, Woodhead Publishing, 2019, pp. 407–426.
[54] H. Rajandas, S. Parimannan, K. Sathasivam, M. Ravichandran, L. Su Yin, A novel FTIR-ATR spectroscopy based technique for the estimation of low-density polyethylene biodegradation, Polym. Test. 31 (8) (2012) 1094–1099.
[55] J.V. Gulmine, P.R. Janissek, H.M. Heise, L. Akcelrud, Polyethylene characterization by FTIR, Polym. Test. 21 (5) (2002) 557–563.
[56] T.S. Tofa, F. Ye, K.L. Kunjali, J. Dutta, Enhanced visible light photodegradation of microplastic fragments with plasmonic platinum/zinc oxide nanorod photocatalysts, Catalysts 9 (10) (2019) 819.
[57] T.H. Ha, J.Y. Jang, Y.B. Cho, H.M. Jeong, B.K. Kim, Maleic anhydride grafted polyethylene powder coated with epoxy resin: a novel reactive hot melt adhesive, J. Appl. Polym. Sci. 116 (1) (2009) 328–332.
[58] M. Sclavons, M. Laurent, J. Devaux, V. Carlier, Maleic anhydride-grafted polypropylene: FTIR study of a model polymer grafted by ene-reaction, Polymer 46 (19) (2005) 8062–8067.
[59] D. Xu, J. Lu, S. Yan, R. Xiao, Aminated EVOH nanofiber membranes for Cr(vi) adsorption from aqueous solution, RSC Adv. 8 (2) (2018) 742–751.
[60] N. Girard-Perier, S. Dorey, F. Gaston, F. Girard, S.R.A. Marque, N. Dupuy, One-year ageing FTIR monitoring of PE/EVOH/PE film after gamma or electron beam irradiation, Polym. Degrad. Stab. 195 (2022).
[61] W. Xu, S. Asai, M. Sumita, Spectroscopic study of ethylene vinyl alcohol copolymer and poly (vinyl alcohol), Sen'i Gakkaishi 53 (5) (1997) 174–182.
[62] J.S. Andre, B. Li, X. Chen, R. Paradkar, B. Walther, C. Feng, C. Tucker, C. Mohler, Z. Chen, Interfacial reaction of a maleic anhydride grafted polyolefin with ethylene vinyl alcohol copolymer at the buried solid/solid interface, Polymer 212 (2021) 123141.
[63] J.M. Lagaron, E. Giménez, J.J. Saura, Degradation of high barrier ethylene–vinyl alcohol copolymer under mild thermal-oxidative conditions studied by thermal analysis and infrared spectroscopy, Polym. Int. 50 (6) (2001) 635–642.
[64] Y. Wang, Y. Shi, W. Shao, Y. Ren, W. Dong, F. Zhang, L.Z. Liu, Crystallization, structures, and properties of different polyolefins with similar grafting degree of maleic anhydride, Polymers 12 (3) (2020).
[65] O. Delgadillo-Velázquez, S.G. Hatzikiriakos, M. Sentmanat, Thermorheological properties of LLDPE/LDPE blends, Rheol. Acta 47 (1) (2007) 19–31.
[66] C. Min, X. Min, L. Yixin, M. Yuezhong, Novel in situ preparation of crosslinked ethylene-vinyl alcohol copolymer foams with propylene carbonate, Mater. Lett. 60 (27) (2006) 3286–3291.
[67] H. Hinsken, S. Moss, J.-R. Pauquet, H. Zweifel, Degradation of polyolefins during melt processing, Polym. Degrad. Stab. 34 (1) (1991) 279–293.
[68] F. Gholami, L. Pakzad, E. Behzadfar, Morphological, interfacial and rheological properties in multilayer polymers: a review, Polymer 208 (2020) 122950.
[69] P. Agrawal, M.H.A. Silva, S.N. Cavalcanti, D.M.G. Freitas, J.P. Araújo, A.D. B. Oliveira, T.J.A. Mélo, Rheological properties of high-density polyethylene/linear low-density polyethylene and high-density polyethylene/low-density polyethylene blends, Polym. Bull. 79 (4) (2021) 2321–2343.
[70] S. Trinkle, C. Friedrich, Van Gurp–Palmen-plot: a way to characterize polydispersity of linear polymers, Rheol. Acta 40 (4) (2001) 322–328.
[71] S. Trinkle, P. Walter, C. Friedrich, Van Gurp–Palmen plot II—Classification of long chain branched polymers by their topology, Rheol. Acta 41 (1–2) (2002) 103–113.
[72] M. van Gurp, J. Palmen, Time-temperature superposition for polymeric blends, Rheol. Bull. 67 (1998) 5–8.
[73] Z. Qian, G.B. McKenna, Expanding the application of the van Gurp–Palmen plot: new insights into polymer melt rheology, Polymer 155 (2018) 208–217.
[74] C.A. Garcia-Franco, D.W. Mead, Rheological and molecular characterization of linear backbone flexible polymers with the Cole–Cole model relaxation spectrum, Rheol. Acta 38 (1) (1999) 34–47.
[75] H. Azizi, I. Ghasemi, M. Karrabi, Controlled-peroxide degradation of polypropylene: rheological properties and prediction of MWD from rheological data, Polym. Test. 27 (5) (2008) 548–554.
[76] S. Rolere, M. Cartault, J. Sainte-Beuve, F. Bonfils, A rheological method exploiting Cole–Cole plot allows gel quantification in natural rubber, Polym. Test. 61 (2017) 378–385.